Analyst

ROYAL SOCIETY OF CHEMISTRY

PAPER

View Article Online
View Journal

Cite this: DOI: 10.1039/c9an02291k

A capacitive DNA sensor for sensitive detection of *Escherichia coli* O157:H7 in potable water based on the *z3276* genetic marker: fabrication and analytical performance†

Rehan Deshmukh,[a] Arun Kumar Prusty,[b] Utpal Roy *‡[a] and Sunil Bhand *‡[b]

We report a label-free biosensor for the detection of *Escherichia coli* O157:H7 ATCC 43895 in potable water using a newly designed DNA sensing probe targeting the *z3276* genetic marker. The surface of indium tin oxide (ITO) was functionalized with the novel sensing probe by covalent coupling using APTES as a crosslinker to fabricate the DNA sensor (dubbed ZEC [*z3276* gene of *E. coli* O157:H7 ATCC 43895]). The electrochemical characterization of the fabricated ZEC sensor was performed using cyclic voltammetry and electrochemical impedance spectroscopy. Atomic force microscopy and scanning electron microscopy revealed significant changes in the surface topographies of the fabricated ZEC sensor chip. Equivalent circuit analyses suggested the capacitive nature of the ZEC sensor chip, which demonstrated a declining trend of the capacitance value from 1.568 μF (Bare ITO) to 1.221 μF (after DNA hybridization). Non-faradaic sensing measurements revealed systematically declining capacitance values upon DNA hybridization, with a 10 min response time at 10 Hz frequency and 10 mV applied potential. The ZEC sensor chip exhibited linearity in the range of 0.5 to 25 pg per 10 mL for *E. coli* O157:H7, with ubiquitous cross-validation of each DNA concentration using quantitative PCR prior to the analyses of real water samples. The limit of detection (LOD) at 95% confidence estimated by logistic regression was 0.1 pg DNA per 10 mL of *E. coli* O157:H7 (equivalent to 13.67 CFU per 10 mL) with a *p*-value of 0.0237. Consequently, the obtained results demonstrate the possible application of the developed ZEC sensor chip for *E. coli* O157:H7 detection in real water samples.

Received 14th November 2019,
Accepted 6th January 2020

DOI: 10.1039/c9an02291k

rsc.li/analyst

1. Introduction

Escherichia coli O157:H7 is a food-and-water-borne pathogen that has been implicated in several outbreaks worldwide in humans as well as in animals and poultry.[1–3] It is estimated that *E. coli* O157:H7 globally causes over 2.8 million acute illnesses annually.[4] Therefore, in order to monitor future outbreaks effectively, it is indispensable to have access to sufficiently rapid and sensitive methods that can be employed for the detection of *E. coli* O157:H7.

To date, many attempts have been made to develop methods for the rapid detection of *E. coli* O157:H7. Traditionally, methodologies for the detection of DNA hybridization have been exploited based on the attachment of different labels to the molecules being investigated. The standard labels utilized in molecular biology studies to evaluate DNA hybridization include fluorescent dyes,[5] redox-active enzymes[6,7] and magnetic particles.[8] For example, when the DNA target sequence is labeled with an appropriate fluorescent tag, fluorescence can be observed with the aid of a fluorescence microscope at the location of complementary hybridization.[9] However, although these methodologies are sensitive, labeling methods are time-consuming, expensive and require sample handling.[10] These labels in a few cases may interfere with the hybridization of two complementary DNA strands.[11] Therefore, there is currently a dire need to develop simple, reliable and inexpensive methods for sensing microbial pathogens. Label-free methodologies have emerged as sensitive yet cost-effective impedimetric tools for the detection of DNA hybridization phenomena.[12] In principle, label-free DNA-based biosensors depend on the alteration of a given quantitative parameter of the transducer, which is influenced by the DNA hybridization phenomenon. Label-free methodologies can proffer tangible information about changes in the physical

[a]Birla institute of Technology and Science, Pilani, Department of Biological Sciences, Goa Campus, NH17B Bypass, Goa 403726, India. E-mail: utpalroy@gmail.com
[b]Birla institute of Technology and Science, Pilani, Department of Chemistry, Goa Campus, NH17B Bypass, Goa 403726, India. E-mail: sunil17_bhand@yahoo.com

†Electronic supplementary information (ESI) available. See DOI: 10.1039/c9an02291k

‡Equal correspondence.

characteristics of the analyte under investigation. EIS can be exploited for DNA hybridization detection, mainly due to its capability to execute label-free detection. EIS can sensitively monitor the variations of the capacitance at the electrode or electrolyte interface when the DNA target complementarily binds with the DNA probe.[11] Faradaic detection of DNA hybridization using EIS necessitates the addition of a redox-active species, such as $[Fe(CN)_6]^{3-/4-}$ or $[Ru(NH_3)_6]^{2+/3+}$; it relies on the variation of the charge transfer resistance between the electrode surface and the solution.[11,13] In contrast, non-faradaic detection is independent of redox-active species. Modification of the surface of the electrode by biomolecules generally leads to changes either in the double layer capacitance embodied between the electrode surface and the solution or the capacitance positioned in the space charge layer at the interface of the semiconducting electrodes.[14] In such cases, a highly sensitive electrode material is required for the purpose of capacitive sensing. Many sensitive materials for electrochemical label-free DNA detection have been reported, such as the use of metals,[15,16] conductive polymers[17,18] and semiconductors.[19,20] In addition to label-free impedimetric DNA sensors, pulsed amperometry and differential pulse voltammetry-based label-free detection of DNA hybridization has been reported.[21,22] However, in the present research, we have developed a capacitive (non-faradaic impedimetric) sensing platform for the detection of *E. coli* O157:H7 which shows higher sensitivity and a lower limit of detection (LOD).

Novel degenerate semiconductor electrodes, such as indium tin oxide (ITO), exhibit prominent characteristics, such as high conductivity and outstanding optical transparency. Notably, these electrodes have received immense attention over the last few decades and have been widely utilized due to their substrate adhesion and electrochemical properties.[23,24] For example, in biosensor development, ITO surfaces have been generally modified with silane monolayer to enable the immobilization of biomolecules, such as amine-terminated DNA probes.[11] The electrodeposition of nano-composites of graphene oxide/iron oxide mixed with chitosan polymer onto the surface of an ITO electrode to covalently immobilize an amine-labeled DNA probe for the detection of *E. coli* 157:H7 was reported.[25] A similar immobilization strategy was explored by Xu *et al.*, who reported the use of chitosan/iron oxide films as a DNA probe-matrix.[26]

The specificity of the DNA probe is extremely important for the detection of microbial pathogens. The open reading frame (ORF) *z3276* has been shown to be a specific and stable genetic marker for *E. coli* O157:H7 detection; it encodes a putative fimbrial protein, as reported elsewhere.[27] Therefore, in the present study, sequences of ORF *z3276* were selected to design the DNA probe using the BLAST software suite of the National Centre for Biotechnology Information (Maryland, USA). An additional challenge confronting the specific detection of *E. coli* O157:H7 in contaminated water sources is to accurately detect low numbers of cells in test samples. Hence, in the present study, we report for the first time a novel DNA-chip impedimetric sensor based on the *z3276* gene, dubbed ZEC (*z3276* gene of *E. coli* O157:H7 ATCC 43895), using an ITO surface modified with an organosilane linker. The DNA probe used for the detection of *E. coli* O157:H7 was further immobilized onto the GA-modified electrode.

The present work is organized as follows: (i) design of a specific DNA probe for sensitive detection of *E. coli* O157:H7 by targeting the *z3276* genetic marker; (ii) characterization of the ZEC sensor chip by electrochemical impedance spectroscopy (EIS), atomic force microscopy (AFM) and scanning electron microscopy (SEM); (iii) capacitive sensing of *E. coli* O157:H7 based on the non-faradaic detection of DNA hybridization signals; and (iv) cross-validation with the qPCR technique.

2. Experimental section

2.1. Materials

ITO slides with a resistivity of 8 to 12 Ω cm^{-1} (Sigma, USA) were used for the fabrication of the ZEC sensor chip. 3-Aminopropyltrimethoxysilane (APTES) and GA were obtained from Thermo Fisher Scientific, USA. All the reagents and buffers were prepared using sterile deionized water. Media for bacterial growth were obtained from HiMedia (Mumbai, India).

2.2. Instrumentation

The EIS studies were performed with a CompactStat measurement station (Ivium Technologies, Netherlands) in a customized three-electrode setup comprising Ag/AgCl electrode as the reference electrode and a platinum wire as the counter electrode. The ITO electrodes were precisely cut with a diamond wire saw to maintain constant dimensions and were used as the working electrodes. All the electrodes were placed on a Teflon holder mounted on a small glass vial of 3 mL capacity for the electrochemical measurements. Cyclic voltammetry (CV) and EIS characterization of the ZEC sensor chip and further capacitance measurements for sensing of *E. coli* O157:H7 ATCC 43895 were performed using the electrochemical instrument mentioned earlier in this section.

2.3. Bacterial strains and culture conditions

The bacterial strains were procured from Microbial Type Culture Collection and Gene Bank (MTCC, India) and American Type Culture Collection (ATCC, US). All bacterial strains, *E. coli* O157:H7 ATCC 43895, *Escherichia coli* MTCC 3221, *Escherichia coli* O78:H11 MTCC 723 and *Bacillus subtilis* MTCC 736 were grown to attain logarithmic phase (Optical Density at 600 nm [OD600], 0.5 to 0.6) in Trypticase Soy Broth (TSB) at 37 °C.

2.4. Spiking of water samples and DNA extraction

E. coli ATCC 43895 cells were grown until they reached the logarithmic phase (OD_{600} 0.5 to 0.6) in TSB. The culture was adjusted to a 0.5 McFarland standard (1% H_2SO_4 v/v, 1.175% $BaCl_2{\cdot}2H_2O$ w/v) to serially dilute it 10 fold in sterile bacterio-

logical saline (0.85% NaCl). An aliquot of 10^{-5} dilution was used to spike 10 mL autoclaved potable water samples. The membrane filtration method was performed as described earlier by Deshmukh *et al.*[28] Following the membrane filtration, the filter was incubated on Difco™ 4-methyl-umbelliferyl-β-D-galactopyranoside and indoxyl-β-D-glucuronide (MI) agar supplemented with 5 μg mL^{-1} cefsulodin (MP Biomedicals, Santa Ana, USA) for 24 ± 2 h at 37 °C. Two colonies of *E. coli* ATCC 43895 were selected from the MI agar plate and subjected to DNA extraction using a NucleoSpin® tissue DNA extraction kit (Macherey-Nagel, Germany) as per the manufacturer's instructions. The DNA concentrations were measured using a NanoDrop™ spectrophotometer (Thermo Fischer Scientific, USA), which yielded 35.1 ng μL^{-1} with an A_{260}/A_{280} ratio of 1.8.

2.5. Design of the primers and probe

DNA probes are of great importance to the success of DNA sensor-based assays; therefore, the primers and probes were designed by constructing alignment of multiple *z3276* sequences obtained from public databases. The PrimerQuest Tool from Integrated DNA Technologies (IDT, Coralville, USA) was employed to choose the candidate primer sequences. The forward primer (from 320 to 340 nucleotides, 5′-AATGGATGCCCTGAAACCTC-3′), the reverse primer (from 417 to 437 nucleotides, 5′-TGAGCTTGCCCTAGAATTG-3′) and the DNA probe (from 372 to 396 nucleotides, 5′-NH_2-$(CH_2)_6$-TAGCCTTACCGCTGACCCATTGTT-3′) were designed to target the *z3276* genetic marker of *E. coli* O157:H7 EDL 933 (GenBank accession number AE005174). The oligonucleotide primers and the aminated DNA probe were synthesized by Integrated DNA Technologies (Coralville, USA). The specificity of the probe was further evaluated using the BLAST suite of software available at the NCBI site (http://blast.ncbi.nlm.nih.gov/Blast.cgi).

2.6. Quantitative PCR (qPCR)

The qPCR amplification reaction was executed by a LightCycler® 96 Real-Time PCR system (Roche Diagnostics, Risch-Rotkreuz, Switzerland) using FastStart Universal SYBR Green Master mix (Roche Diagnostics). 5 μL of an appropriately diluted concentration of the template was added to a 20 μL qPCR reaction containing 50 pmol of forward and reverse primers, 3.3 μg μL^{-1} bovine serum albumin, and 2× FastStart Universal SYBR Green Master mix.[28] A volume of 2 μL of PCR-grade water (Roche Diagnostics) was used to adjust the volume of the PCR reaction. In each experiment, 5 μL of nuclease-free water was added to a PCR reaction mixture to serve as a no-template control (NTC). The following PCR amplification conditions were used: initial thermal cycling for 180 seconds at 95 °C followed by 40 cycles of 30 s at 95 °C, 30 s at 58 °C, and 30 s at 72 °C. The specificity of the assay was examined by melting temperature (T_m) profiles produced for the amplicons over a temperature range of 65 °C to 95 °C.[29] The qPCR calibration curve was generated by amplification of purified DNA of *E. coli* O157:H7 ATCC 43895 in the 0.1 picogram (pg) to 50 pg range, wherein the experiments were performed in triplicate. The cycle of quantitation (C_q) values for each amplicon was plotted against the log of each DNA concentration used. Purification of PCR products was carried out using a PCR Clean-Up kit as per the manufacturer's instructions (APS Lifetech, Pune, India).

2.7. Fabrication of ZEC sensor chip

Prior to surface modification, the Bare ITO chip was initially cleaned by treating it with basic piranha solution ($NH_4OH : H_2O_2 : H_2O$ in a 1 : 1 : 5 ratio, respectively) for 20 min at 80 °C. Subsequently, it was rinsed extensively with deionized water and completely dried under a nitrogen atmosphere. For the silanization process, the Bare ITO chip was incubated for 1 hour in 1% APTES prepared in 95% ethanol to form –Si–O– bonds.[11] After incubation, the APTES-coated ITO chip was washed thoroughly using absolute ethanol to remove the excess unbound organosilane from the ITO surface. The APTES-coated chip was denoted as S-ITO. Then, the S-ITO chip was immersed in 10% GA for 2 hours to form the GA film through amine-aldehyde bonds. The GA-coated chip was denoted as G-ITO. The G-ITO chip was then washed sufficiently with ultrapure water to wash off any unbound GA. The area on the G-ITO surface was controlled using insulation adhesive tape, as shown in Fig. 1. The aminated DNA probe (20 ng μL^{-1}) was then immobilized onto the G-ITO chip in an area of approximately 3.14 mm^2 (Fig. 1) and incubated for 2 hours at room temperature in a humid chamber. The unbound probe was removed by thorough washing with phosphate-buffered saline (PBS, 10 mM, pH 7.4). The DNA probes were reduced and stabilized as described by Le *at al.*[11] The chip after immobilization with DNA probe was designated as the ZEC sensor chip. The hybridization was carried out using genomic DNA (denatured at 95 °C) for 5 min with an immobilized *z3276* DNA probe onto the ZEC sensor chip surface. After hybridization, the sensor was washed with copious amounts of PBS to remove the unbound single-stranded DNA (ssDNA). Schematics of the ZEC sensor chip fabrication and the electrochemical measurement setup have been outlined in Fig. 1. Different types of DNA targets were purified from cells of *E. coli* MTCC 3221, *E. coli* O78:H11 MTCC 723 and *B. subtilis* MTCC 736 in order to study the specificity of the fabricated ZEC sensor chip. The LOD was calculated using the equation LOD = 3 × sd/m, where sd and m denote the standard deviation and the slope of the calibration curve, respectively.[30]

2.8. Characterization of the ZEC sensor chip

For electrochemical characterization of the ZEC sensor chip, impedance measurements were performed for (I) Bare ITO; (II) S-ITO; (III) G-ITO and (IV) the ZEC sensor chip before and (V) after DNA hybridization. The electrolyte employed methodically was PBS solution containing no DNA target. A laboratory-made electrochemical cell consisting of a three-electrode setup was used in which the liquid volume was 700 μL. The ZEC sensor chip served the purpose of the working electrode. The reference and counter electrodes were Ag/AgCl and platinum

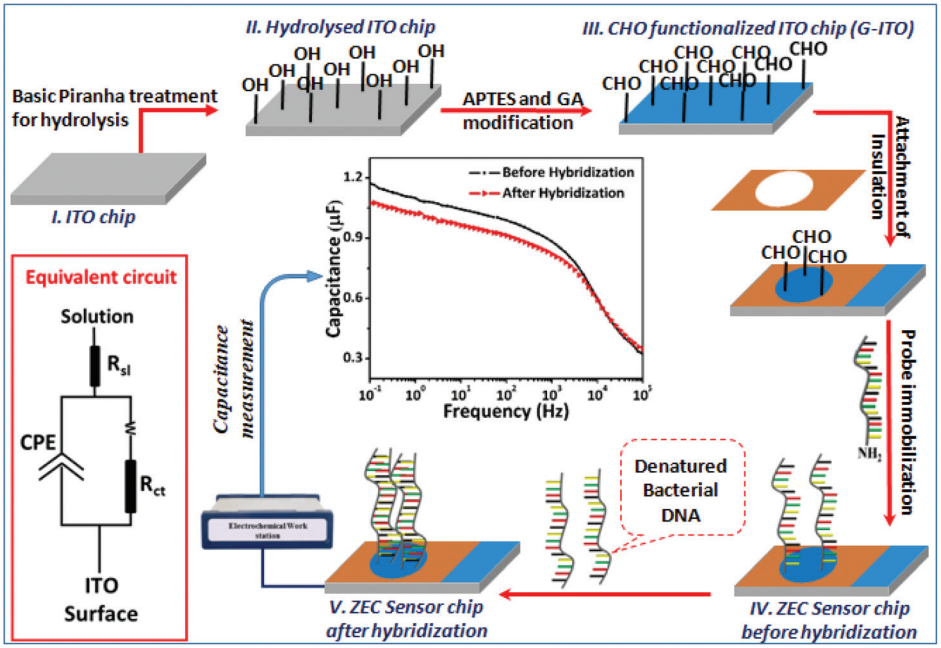

Fig. 1 Schematics representing the different steps of ZEC sensor chip fabrication and the capacitance measurement of DNA from *E. coli* O157:H7 cells. CPE, double layer capacitance; *W*, Warburg resistance; R_{sl}, solution resistance; and R_{ct}, charge transfer resistance.

wire, respectively. The EIS response signals were quantitatively measured between 10^{-1} and 10^{5} Hz with an applied alternating potential of 10 mV peak to peak. This work was performed to develop a capacitive ZEC sensor chip without the use of labels based on the principle of capacitive sensing reported elsewhere.[31,32] Surface topographical studies at different stages of sensor chip fabrication were performed using AFM (NTEGRA Prima, NT-MDT, Russia) and SEM (Quanta 250 FEG, Thermo Fischer Scientific, USA), both at Birla Institute of Technology and Science, Pilani, Goa Campus (Goa, India). For the AFM studies, the fabricated chips, *viz.*, Bare ITO, S-ITO, G-ITO, and ZEC sensor chips before and after DNA hybridization, were scanned in an area of 3 μm^2 in a semi-contact mode. Data analyses were performed using the Nova software suite (NTEGRA Prima, NT-MDT, Russia). For SEM studies, Bare ITO and the ZEC sensor chips before and after DNA hybridization were subjected to sputter coating (Leica EM ACE600, UK) with gold/palladium. The SEM imaging of the fabricated ZEC sensor chip was executed using a Quanta 250 FEG at 400 000× magnification. Attenuated total reflection Fourier-transform infrared spectroscopy (ATRFT-IR) analyses for the ZEC sensor chips before and after hybridization with complementary DNA were performed using IRAffinity-1S (SHIMADZU, Japan).

2.9. Determination of pinholes

The pinholes present on the surfaces of S-ITO, G-ITO, and the ZEC sensor before and after hybridization with ssDNA were calculated from the experimentally obtained EIS data using 1 mM $[Fe(CN)_6]^{3-/4-}$ prepared in 10 mM PBS. The charge transfer resistances (R_{ct}) of the ZEC sensor chip at different stages of fabrication were calculated by fitting the EIS data, as shown in the equivalent circuit (Fig. 1). The fractional coverage area (FA) of each fabricated sensor chip was calculated using the equation reported by Campuzano *et al.*:[33]

$$FA = 1 - \frac{R_{ct}(\text{Bare ITO chip})}{R_{ct}(\text{Modified ITO chip})}$$

(1–FA) x 100 denotes the percentage of pinholes present on the modified ITO chip surface.[33,34]

2.10. Statistical analyses

All individual results were recorded and statistical significances were calculated using Microsoft Excel 2007 software (Microsoft Corporation; Redmond, WA, USA). When the two-sided *p*-value was less than 0.05, we concluded that there was a significant difference between the two recorded experimental values. All the graphs were plotted using OriginPro 8 SRO software (OriginLab Corporation, Northampton, MA, USA).

3. Results and discussion

3.1. Electrochemical analyses for the study of the capacitive properties of the ZEC sensor chip

The capacitive natures of the Bare ITO, S-ITO, G-ITO and ZEC sensor chips were evaluated electrochemically using direct current (DC) and alternating current (AC) bias conditions. The DC and AC analyses of the ZEC sensor chip were performed using CV and EIS techniques, respectively. Both these methods were applied to study the capacitive behavior by analyzing different parameters, such as resistance, relative permittivity, impedance, phase, and capacitance. To investigate these para-

meters, an electrochemical cell connected to an analyzer was used. DC analyses were performed to study the insulating nature of the ZEC sensor chip surface, where CV sweeps between −0.4 V and +0.4 V were applied and the resulting voltammograms were recorded. The voltammograms demonstrated the resistance offered by the various chip surfaces to electron movement, proving the insulating nature of the fabricated sensor chip surface. The Bare ITO chip showed well-defined redox peaks of the redox couple, whereas no such peaks were observed for the G-ITO or ZEC sensor chips (ESI Fig. S1†).[35]

The capacitive behavior of the sensor chips, namely Bare ITO, S-ITO, G-ITO, and the ZEC sensor chip at various stages of fabrication, was further confirmed by EIS studies based on analyses of the impedance (Fig. 2A) and phase curves (Fig. 2B) of the Bode plots. The impedance analyses showed a slope of −0.9 for Bare ITO and a slope of −0.87 for S-ITO, which were observed to be lower than the slopes of G-ITO (−0.92) and the ZEC sensor chip (−0.94) (Fig. 2A). The slope values nearing −1 for the G-ITO and ZEC sensor chips indicate their insulating nature and approach the ideal Randles equivalent circuit for capacitive behavior.[36] Moreover, these improved slopes for the G-ITO and ZEC sensor chips along with the higher values of impedance for Bare ITO and S-ITO (Fig. 2A) reveal the insulating nature of the ZEC sensor chip[37] and its suitability for capacitance-based sensing of *E. coli* O157:H7. Interestingly, the same capacitive behavior of the fabricated ZEC sensor chip was also evident from the phase-change curves, as shown in Fig. 2B. It was evident that the ZEC sensor chip exhibited the highest phase (87°) at 10 Hz, whereas the G-ITO chip showed a phase value of 85.82° (Fig. 2B), higher than what was observed for Bare ITO (85.34°); this indicates nearly ideal capacitive behavior of the ZEC sensor at 10 Hz. The recorded phase value for S-ITO was 84.94°. The capacitive properties of the Bare ITO, S-ITO, G-ITO, and ZEC sensor chip surfaces were further investigated using the relative permittivity variations with respect to frequency, as shown in Fig. 2C. It was observed that S-ITO showed higher relative permittivity than Bare ITO, G-ITO and the ZEC sensor chip, which can be attributed to the presence of $-NH_2$ groups in APTES. However, the G-ITO and ZEC sensor chips showed lower permittivity; this, in turn, confirmed their insulating nature under DC bias studies (Fig. 2C). The capacitive properties of the ZEC sensor chip were further studied using capacitance variation plots, as shown in Fig. 2D.

The capacitance value is directly proportional to the relative permittivity; hence, similar capacitance variations were

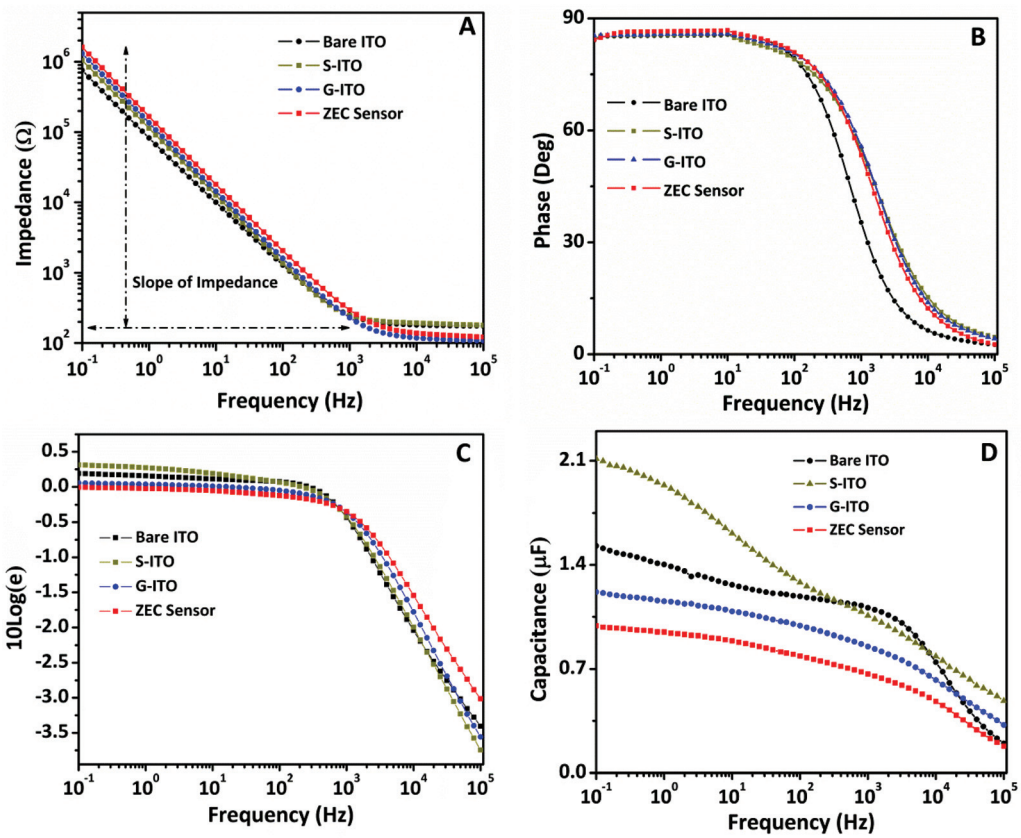

Fig. 2 Characterization of the fabricated electrodes for the development of a ZEC sensor chip for the detection of *E. coli* O157:H7 ATCC 43895. Impedance components of the Bode plots (A); phase components of the Bode plots (B); relative permittivity variation plots (C); and capacitance variation plot (D) corresponding to electrodes at different stages of sensor fabrication recorded in PBS using EIS. A frequency range of 10^{-1} to 10^{5} Hz was used with an applied potential of 10 mV.

observed for all the fabricated chips except for S-ITO. In the cases of the Bare ITO, G-ITO and ZEC sensor chips, the capacitance followed a descending trend and was found to be directly proportional to the relative permittivity, as illustrated in Fig. 2C. Even with the descending trend of capacitance value, we did not observe a rapid variation of capacitance over a wide range of frequency; hence, these observations indicate the suitability of the ZEC sensor chip for capacitance-based biosensor development. In addition, analyses of the admittance plots further suggested capacitive behavior corresponding to the ZEC sensor chip at different steps of fabrication (ESI Fig. S2†). Fig. S2A (ESI†) shows the variations of the real and imaginary parts of the admittance, which correspond to the resistive and capacitive effects of Bare ITO in the frequency range of 10^{-1} to 10^{5} Hz. The imaginary part was above the real part, and the capacitive behavior was found to overcome the resistive behavior only after 680 Hz in the case of the Bare ITO chip. In the case of S-ITO, the imaginary part was above the real part after 714 Hz (ESI Fig. S2B†); this suggests the presence of pinholes, which allow the resistive current component to dominate the capacitive current component. Further improvements were observed in the cases of the G-ITO and ZEC sensor chips, as shown in Fig. S2C and Fig. S2D (ESI†). Both the figures show dominance of the capacitive component over the resistive component in a wide frequency range, starting from 1197 Hz and 1640 Hz, respectively; this indicates the suitability of these fabricated chips for the purpose of capacitive sensing. The ratios of the imaginary and real components of admittance corresponding to the ZEC sensor chip were calculated at different steps of fabrication in the given frequency range, as shown in Table 1. In the case of G-ITO, it was found that at 10 Hz, the ratio of 22.48 was higher than at the other frequencies; this confirms the higher phase angle variation at 10 Hz compared to other frequencies, as shown in Fig. 2B. Moreover, the ZEC sensor chip had the highest ratio of admittance (24.8621) over Bare ITO (14.4728), S-ITO (10.8831) and G-ITO (22.48) at 10 Hz in the whole frequency range (Table 1).

These ratios of the imaginary to the real part of the admittance values indicate that at 10 Hz, the capacitive reactance value dominated the resistance value; this confirms the highest capacitive effect of the ZEC sensor chip in the frequency range tested (Table 1; ESI Fig. S2†). Hence, 10 Hz was taken as the working frequency for the desired capacitance measurements.

The equivalent circuit parameters corresponding to the proposed model were calculated at each stage of sensor fabrication, as shown in Table 2. In the proposed model, R_{ct} represents the charge transfer resistance, CPE (constant phase element) denotes the double layer capacitance, w indicates the finite length Warburg impedance, and R_{sl} represents the solution resistance at the interface of the ZEC sensor chip surface and the test solution (PBS). The proposed model was the best fitted model when calculating the equivalent circuit parameters by optimizing the phase and the magnitude of the Bode plots using Ivium software. Fig. S3A–S3J (ESI†) depicts the circuit fitting plots employed in the EIS studies. The equivalent circuit parameter, charge transfer resistance (R_{ct}), showed a change in value from 4.112×10^{6} Ω for Bare ITO to 3.275×10^{7} Ω and 2.025×10^{8} Ω for G-ITO and the ZEC sensor chip, respectively, confirming the surface modification by GA and the attachment of the DNA probe onto the ZEC sensor chip. A further increase in R_{ct} was observed after DNA hybridization with the ZEC sensor chip (Table 2). This increase of R_{ct} precisely indicates the highly insulating nature of the ZEC sensor chip. However, in the case of S-ITO, the R_{ct} value was found to decrease to 1.692×10^{3} Ω compared to Bare ITO, which may result from the $-NH_2$ groups of APTES.

The CPE has two components, Q_0 and n. An n value greater than 0.75 is an indicator of the closeness of the CPE to an ideal capacitor. The capacitance values C corresponding to

Table 1 Ratios of the imaginary to the real part of the admittance values for Bare ITO, S-ITO, G-ITO, and the ZEC sensor at different frequencies

Frequency (Hz)	10^5	10^4	10^3	10^2	10^1	10^0
Bare ITO	0.04474	0.1116	0.7090	5.2829	14.4768	13.180
S-ITO	0.0201	0.1170	0.7741	3.4738	10.8831	6.1534
G-ITO	0.07296	0.8974	1.4666	1.4666	22.48	13.8545
ZEC sensor	0.02	0.1664	1.15	5.1807	24.8621	14.6348

Table 2 Equivalent circuit fitted parameter values obtained for the ZEC sensor chip using EIS data in 10 mM PBS

Characteristic	R_{sl} (Ω)	R_{ct} (Ω)	Q (Constant phase element)		C ($(Q_0 \times R_{ct})^{1/n}/R_{ct}$) (μF)	Warburg impedance (W) (1/Ohm $Hz^{0.5}$)
			Q_0 (S)	n		
Bare ITO	1.879×10^{2}	4.112×10^{6}	1.472×10^{-6}	0.9655	1.568	4.117×10^{-8}
S-ITO	1.581×10^{2}	1.692×10^{3}	94.92×10^{-6}	0.9899	93.165	3.805×10^{-8}
G-ITO	1.304×10^{2}	3.275×10^{7}	1.031×10^{-6}	0.9136	1.438	1.148×10^{-8}
ZEC sensor	1.558×10^{2}	2.025×10^{8}	1.177×10^{-6}	0.9799	1.316	1.762×10^{-8}
After hybridization with DNA	1.614×10^{2}	5.652×10^{8}	1.063×10^{-6}	0.9788	1.221	3.134×10^{-8}

CPE were calculated by the formula given in Table 2. The fitted values for CPE at different stages of ZEC sensor chip fabrication indicate that the n value at each stage was higher than 0.75 and approached the ideal value of 1. The closeness of n to 1 indicates that the behavior of the ZEC sensor chip surface approaches the behavior of an ideal capacitor. The capacitance values calculated from the CPE at each stage of sensor fabrication are shown in Table 2. A decrease in the net capacitance value was noted for the fabricated ZEC sensor chip (Table 2). The increase in capacitance for the S-ITO chip (93.165 μF) over the capacitance value of the Bare ITO chip (1.568 μF) distinctly indicates the surface modification of B-ITO with silane.

A drastic change in the capacitance values from S-ITO to G-ITO was observed, with changes in Q_0 (S) from 94.92×10^{-6} to 1.031×10^{-6}, respectively. This change shows that the surface modification with GA increased the insulation of the surface (the dielectric property). When comparing the Q_0 and n values of G-ITO and the ZEC sensor chip, it was observed that there was no significant change in Q_0 but there was a considerable change in the n value; this indicates the ideal capacitive nature of the ZEC sensor chip. Furthermore, the decline in the net capacitance value of the ZEC sensor chip to 1.316 μF over the G-ITO chip (1.438 μF) confirmed the binding of the DNA probe; this decline in capacitance can be attributed to the increased value of R_{ct} in the case of the ZEC sensor chip. Ramanavicius *et al.* (2010) reported a pyrrole-based system to develop an impedimetric immunosensor wherein the equivalent circuit analysis was performed by taking the CPE as a component of the modelled circuit. The stepwise modification in the pyrrole-based immunosensor development was studied by observing the variation in the CPE parameters. The variations of the CPE and n values clearly demonstrated the layer-by-layer modification of the developed impedimetric immunosensor.[38] Similar trends in the variation of the n and Q_0 values were observed here, which confirms the applicability of the modelled equivalent circuit proposed in the present investigation.

Further, the insulating behavior of the fabricated ZEC sensor chip suitable for capacitive sensing was confirmed by studying the % of pinholes present on the sensor chip surface, which may disrupt the capacitive sensing. The transducer layer should be thin, insulating and devoid of pinholes. A surface with pinholes may short-circuit the system and, hence, decrease the effectiveness of the capacitive sensing of analytes.[36] For the determination of the % pinholes, the R_{ct} values for the ZEC sensor chip at each stage of fabrication were calculated, as shown in Table 3. The electrolyte (PBS) could access the ITO surface through the pinholes. Pinholes probably appear as a result of flawed adsorption of the monolayers onto the sensor chip surface during the self-assembly step or loss of the monolayers during washing or reuse.[33] Therefore, it is evident from the % pinholes measurements that the Bare ITO chip surface was successfully coated with APTES, GA, and the DNA probe. The percentages of pinholes demonstrated that due to the immobilization of the DNA probe, the pinholes present on the ZEC sensor chip decreased to 25% compared with the pinholes on G-ITO. Moreover, in the case of the ZEC sensor chip hybridized with DNA, the percentage of pinholes further declined to 8% compared to the pinholes present on the ZEC sensor chip (Table 3). These results indicate that GA and the immobilized DNA probe behaved as ionic insulators and, thus, rendered the chip virtually defect-free. However, in the case of the S-ITO chip, we observed very high % pinholes and a negative value for the fractional coverage area (−0.9553), as shown in Table 3. The fractional coverage area cannot be a negative value. However, this may have resulted from the presence of the $-NH_2$ groups of APTES, which may have led to the increased flow of electrons at the chip interface, as observed in Fig. S1 (ESI†). Hence, the R_{ct} value for the S-ITO chip concomitantly declined (1.187×10^4 Ω) compared with the R_{ct} value of the Bare ITO chip (2.321×10^4 Ω) (Table 3).

Table 3 Characterization of the ZEC sensor chip based on the fractional coverage area and percentage of pinholes calculated by EIS data using 1 mM $[Fe(CN)_6]^{3-/4-}$ prepared in 10 mM PBS. It can be observed that the R_{ct} (Ω) value increased after the fabrication of each electrode chip and the % pinholes tended to decline

Characteristics	Charge transfer resistance (R_{ct})	FA	% pinholes
Bare ITO	2.321×10^4 Ω	Reference	Reference
S-ITO	1.187×10^4 Ω	−0.9553	195.53
G-ITO	1.137×10^6 Ω	0.9795	2.05
ZEC sensor	1.501×10^6 Ω	0.9845	1.55
After hybridization with DNA	1.595×10^6 Ω	0.9854	1.46

3.2. AFM and SEM analyses for surface topography studies of the ZEC sensor chip

The numerical data for the surface topographies of Bare ITO, S-ITO, G-ITO, and the ZEC sensor chips before and after hybridization with DNA targets were studied using AFM in semi-contact mode and are shown in Table S1 (ESI†).

Notably, the AFM studies revealed the granular structure of the ITO surface, with an average roughness of 1.40293 nm (Fig. 3A). In addition, changes in the surface topographies of the S-ITO chip (Fig. 3B), G-ITO chip (Fig. 3C) and ZEC sensor chip (Fig. 3D) were observed, indicating the subsequent modification of the ITO surface. After silanization, a smooth surface of S-ITO was obtained, with an average roughness of 0.26 nm. This can be attributed to the formation of a thin APTES film on the ITO surface *via* –Si–O– bond formation (Fig. 3B). Moreover, after GA attachment, the average roughness of the G-ITO chip surface increased to 0.83 nm, as depicted in Fig. 3C. It should be noted that the average roughness of the ZEC sensor chip surface increased to 1.27 nm upon probe immobilization, which can be attributed to the immobilization of a well-aligned layer of the aminated DNA probe on the fabricated ZEC sensor chip surface (Fig. 3D). The average surface roughness and average height after hybridization with ssDNA were recorded as 2.04 nm and 9.02 nm, respectively; this indicates that the ssDNA hybridized with the immobilized DNA probe present on the ZEC sensor chip surface (Fig. 3E).

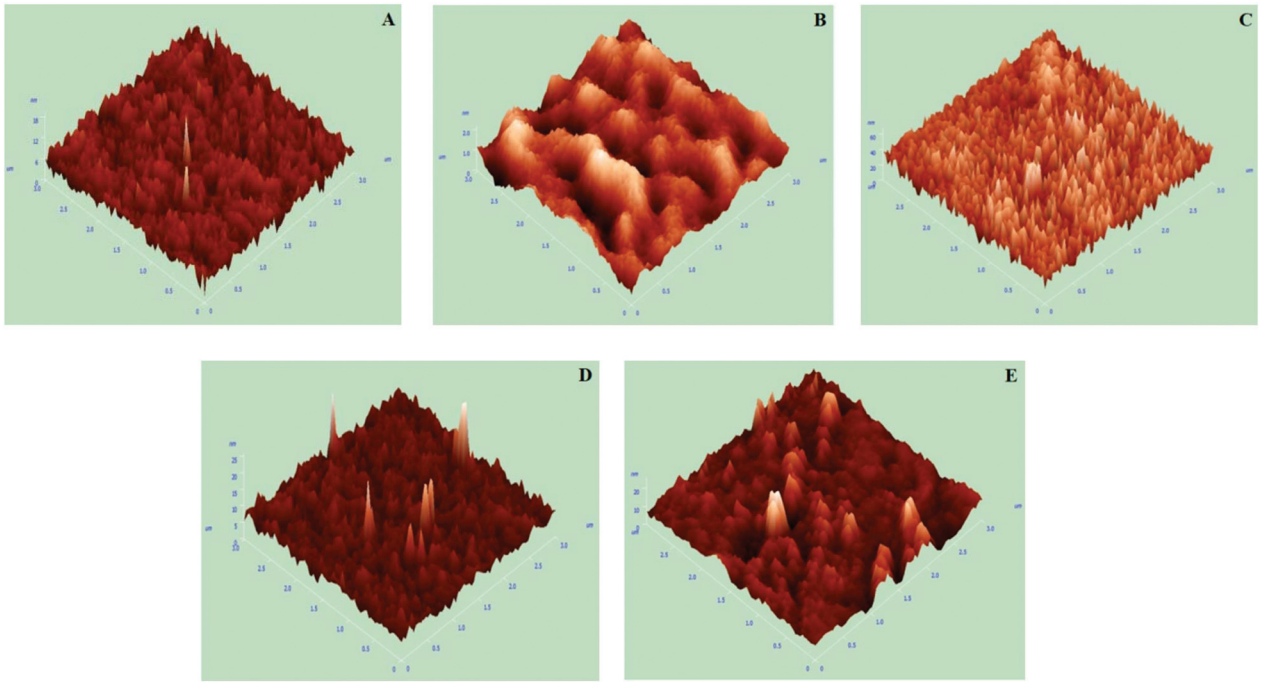

Fig. 3 Characterization of the surface topographies of the ZEC sensor chip using AFM. The AFM images were scanned in a 3 μm^2 area using semi-contact mode in air for the Bare ITO chip surface (A); S-ITO chip surface (B); G-ITO chip surface (C); the ZEC sensor chip surface before hybridization (D); and the ZEC sensor chip surface after hybridization (E) with *E. coli* O157:H7 DNA.

SEM images demonstrated the surface morphologies of the Bare ITO chip, ZEC sensor chip, and ZEC sensor chip hybridized with the DNA of *E. coli* O157:H7 cells (ESI Fig. S5†). Fig. S5A (ESI†) shows rugged grains similar to the structures visible on the surface of the Bare ITO chip. Upon DNA probe immobilization on the G-ITO chip, it was observed that the two-dimensional structure contained smooth stacking layers, indicating apparently uniform attachment of the DNA probe (ESI Fig. S5B†); this is also evident from the % pinholes determination (Table 3). Moreover, DNA hybridization could be clearly visualized on the ZEC sensor, as shown in Fig. S5C (ESI†), where the arrow indicates the unhybridized region on the ZEC sensor.

3.3. ATR FT-IR studies

The ATR FT-IR spectrum of the ZEC sensor chip showed peaks at 781, 884, 959, 1058, 1215, 1275, 1370, 1424, 1482, 1535, 1640, 1690, 1749, and 3383 cm^{-1}, demonstrating the characteristic functional groups of DNA.[39,40] ATR FT-IR spectrum of the ZEC sensor chip after DNA hybridization exhibited similar peaks for different bases, with enhanced peak intensities (Fig. 4).

The peaks observed at 1424, 1640, 1535 and 1749 cm^{-1} characterize the presence of cytosine, thymine, adenine, and guanine, respectively. The peaks at 884 to 781 cm^{-1} correspond to sugar-phosphate and deoxyribose ring vibrations, respectively. In addition, 1215 to 959 cm^{-1} represent the asymmetric and symmetric PO_4^- groups of the phosphodiester deoxyribose backbone. The peaks at 1275, 1525, 1640 and 3383 cm^{-1} can be attributed to N–H stretching and bending of pyrimidine and purine rings. The peaks at 1779 to 1482 cm^{-1}

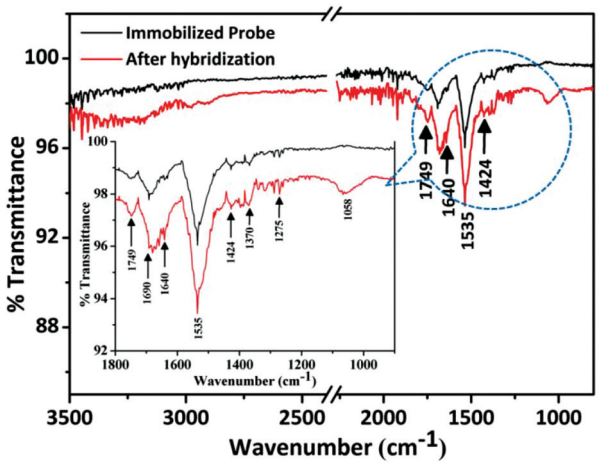

Fig. 4 ATR FT-IR spectra of the ZEC sensor chip before and after hybridization with complementary *z3276* DNA from cells of *E. coli* O157:H7.

indicate the C═N, C═O, and C═C stretching and the exocyclic-NH_2 vibration of DNA bases. These observations corroborate the DNA probe immobilization and hybridization with *E. coli* O157:H7 DNA.

3.4. Capacitance-based detection of *E. coli* ATCC 43895

Using EIS, capacitance-based signals were recorded for different DNA concentrations in the range of 0.1 to 50 pg per 10 mL after baseline measurements in PBS without the DNA

target. A declining trend in capacitance value for each DNA concentration was observed, as shown in Fig. 5A. This decline in capacitance value indicates the hybridization of each complementary DNA target with the DNA probe, except for the 50 pg per 10 mL DNA concentration, which may be due to saturation of the DNA probe at this concentration. In addition, the relative permittivity variation exhibited a declining trend of the dielectric property for each DNA target concentration used, which reinforces the obtained result of the declining trend of capacitance value for each DNA target (ESI Fig. S6A†). Together, these observations suggest desirable capacitive behavior of the fabricated ZEC sensor chip for the detection of *E. coli* O157:H7. The capacitance change response was recorded for various concentrations of DNA targets in the 0.1 to 25 pg per 10 mL range, as shown in Fig. 5B. The fabricated ZEC sensor chip exhibited a linear response in the 0.5 to 25 pg per 10 mL range, with a coefficient of determination (R^2) of 0.971. Similarly, the relative permittivity change response supported the results obtained for the capacitance change response for DNA target concentrations over the 0.1 to 25 pg per 10 mL range; the capacitance change followed a descending trend and was found to be directly proportional to the relative permittivity (ESI Fig. S6B†).

However, the low infective dose of *E. coli* O157:H7 requires the advancement of sensors with lower limits of detection.[41] Wang *et al.* reported a LOD of 150 CFU mL^{-1} for *E. coli* O157:H7 using electrodeposition of gold nanoparticles onto a graphene oxide-modified paper electrode for physisorption of a polyclonal antibody.[42] A similar impedimetric immunosensor for *E. coli* O157:H7 was reported by Wan *et al.* based on gold nanoparticles with a LOD of 100 CFU mL^{-1}.[43] The use of gold nanoparticles modified with thiolated protein G for the detection of *E. coli* O157:H7 with a LOD of 48 CFU mL^{-1} was reported by Lin *et al.*[44] Ruan *et al.* reported an impedimetric *E. coli* O157:H7 immunosensor with a LOD of 6×10^3 CFU mL^{-1} using surface immobilization of antibodies onto ITO electrodes.[45] Similarly, Yang *et al.* reported an impedimetric immunosensor for rapid detection of *E. coli* O157:H7 with a LOD of 10^6 CFU mL^{-1} using anti-*E. coli* antibodies immobilized onto an ITO interdigitated array microelectrode.[46] In comparison, in the present work, a much lower LOD of 13.67 CFU per 10 mL (equivalent to 0.1 pg DNA) for *E. coli*

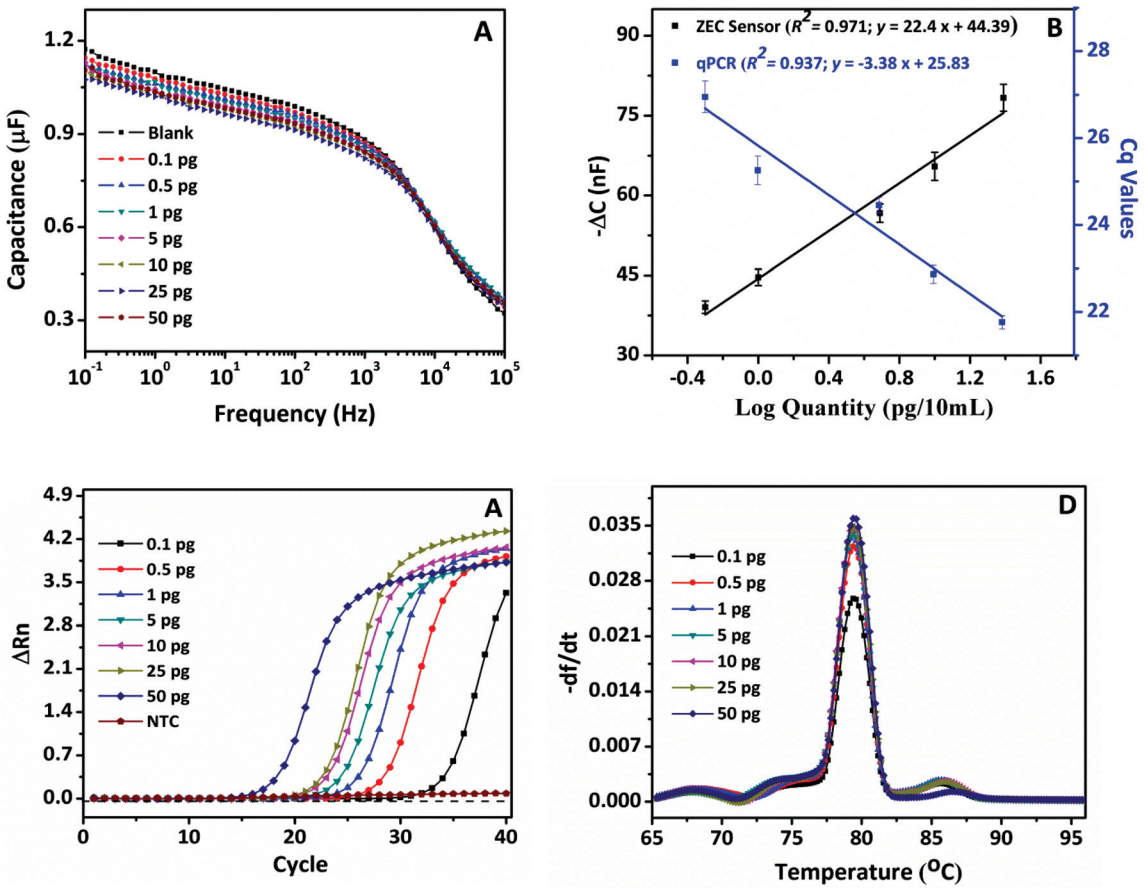

Fig. 5 Capacitance-based detection of *E. coli* O157:H7 using EIS and its validation by qPCR. Capacitance variation plots for different analyte concentrations (pg per 10 mL) recorded in PBS (A); relationships between the capacitance and C_q value for 0.5, 1, 5, 10 and 25 pg per 10 mL analyte concentrations in PBS (B); and validation of the capacitance-based sensing of *E. coli* O157:H7 by qPCR using the amplification curves (C) and melting curves (D) for 0.1, 0.5, 1, 5, 10, 25 and 50 pg DNA per PCR reaction. ΔR_n, fluorescence intensity change; NTC, no-template control; and $-df/dt$, fluorescence per unit temperature.

O157:H7 was obtained using the ZEC sensor chip, with a 10 min response time at the working frequency of 10 Hz and 10 mV applied AC potential. The sensitivity of the ZEC sensor chip can be attributed to the specificity of the *z3276* DNA probe. In addition, all the studies cited above utilized $[Fe(CN)_6]^{3-/4-}$ as the redox couple, whereas no redox probe has been used in our work. Moreover, in the three-electrode system, there is no potential drop across the reference electrode; hence, an accurate potential develops at the working electrode against the counter electrode, so no electrical signal masking is observed for the capacitance measurements.[47] Because of the three-electrode system and the insulating nature[47] of the ZEC sensor chip, no short-circuiting phenomenon was observed in the capacitance measurements.

The performance of the capacitance-based estimation of DNA hybridization for detection of *E. coli* O157:H7 ATCC 43895 was further validated by qPCR based on the amplification signals obtained for each DNA target (Fig. 5C). The melt curve analysis of each DNA target indicated that the qPCR amplification was highly specific for the detection of *E. coli* O157:H7 ATCC 43895 (Fig. 5D).

Analyses of the melt peaks are also crucial in order to obtain reproducible amplification of target genes without non-specific PCR product formation.[28,48] Moreover, the sensitivity of the ZEC sensor chip was validated using the PCR calibration curve (Fig. 5B) to detect each DNA target concentration by qPCR (R^2 = 0.937). For this purpose, the capacitance change response of each DNA target was analyzed using the same measurement settings. The lowest concentration of DNA (0.1 pg; average C_q, 32.34 ± 0.91) amplified by qPCR exhibited a capacitance change response of 26.65 ± 2.1 nF (0.1 pg per 10 mL); the capacitance change response followed a descending trend with increasing DNA concentration, as validated based on the C_q values for 0.5, 1, 5, 10, and 25 pg DNA per 10 mL concentrations (Fig. 5B). Fig. 5B illustrates that the capacitance change response and the C_q value have a linear relationship. These results demonstrate that the fabricated ZEC sensor chip possesses better linearity and a better quantification limit compared with the previously reported *E. coli* O157:H7 sensors (ESI Table S2†). Moreover, the sensor chips tested from different batches of experiments showed variations of <5%, indicating acceptable repeatability.

3.5. Recovery rate and analyses of real water samples

To evaluate the recovery rate and efficiency of the ZEC sensor chip, *E. coli* O157:H7 cells were spiked in tap water samples. *E. coli* cells from 15 to 150 CFU per 10 mL were always detected by the ZEC sensor chip in each spiking experiment. All water samples were found to be negative for *z3276* gene detection prior to the spiking experiments using the qPCR method. Bacterial cells were always detected by the ZEC sensor chip at concentrations as low as 13.67 ± 1.15 CFU per 10 mL, as validated by qPCR and average bacterial counts on MI agar plates (Table 4).[25] The recovery rates were found to be 98.33%, 96.66% and 96.43% for 15, 75 and 150 CFU per 10 mL of *E. coli* O157:H7, respectively, as shown in Table 4. The number of CFU tested by the ZEC sensor chip was calculated by dividing the number of CFU obtained on MI agar by 50 (total volume eluted after DNA extraction) because only 10 μL of the purified DNA sample was tested by the ZEC sensor chip. The LOD at 95% confidence for *E. coli* O157:H7 detection estimated by logistic regression was 13.67 CFU per 10 mL (equivalent to 0.1 pg DNA of *E. coli* O157:H7; *p*-value of 0.0237).

3.6. Specificity analysis of the ZEC sensor chip

The analytical specificity of the fabricated ZEC sensor chip showed that the DNA probe was highly specific for the identification of *E. coli* O157:H7 (Fig. 6). However, a small capacitance change response of 3.3 ± 0.75 nF was observed for *E. coli* MTCC 3221 against a 0.1 pg per 10 mL (average, 26.65 ± 2.1

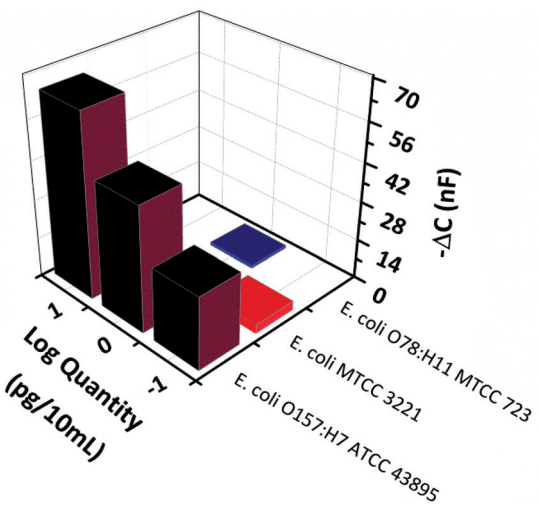

Fig. 6 Histogram of cross-reactivity for 0.1, 1 and 10 pg per 10 mL analyte concentrations of *E. coli* O157:H7 ATCC 43895 in PBS with DNA from *E. coli* MTCC 3221 and *E. coli* O78:H11 MTCC 723.

Table 4 Spiking of potable water samples and determination of the recovery rate for the detection of *E. coli* O157:H7. The ZEC sensor chip could detect as few as 13.67 ± 1.15 CFU of *E. coli* O157:H7 per 10 mL of water sample, with a recovery rate of 98.33%

Target *E. coli* O157:H7 (CFU per 10 mL)[a]	Approximate DNA equivalent of target *E. coli* O157:H7 (pg)	Average *E. coli* O157:H7 count on MI agar (CFU per 10 mL) ± SD	CFU/qPCR reaction[b]	CFU/ZEC Sensor[c]	Recovery (%)
15	**0.1**	13.67 ± 1.15	1.48	2.96	98.33
75	**0.5**	70.33 ± 1.53	7.19	14.38	96.66
150	**1**	142 ± 2.65	14.47	28.94	96.43

[a] n = 3. [b] Number of *E. coli* CFU/qPCR reaction was estimated to be 5/50 of the average *E. coli* O157:H7 count on MI agar.[28] [c] Number of *E. coli* CFU/ZEC sensor chip was estimated to be 10/50 of the average *E. coli* O157:H7 count on MI agar.[28]

nF) DNA concentration of *E. coli* O157:H7 ATCC 43895. Similarly, a negligible capacitance change response of 1.06 ± 0.25 nF was noted for *E. coli* O78:H11 MTCC 723 against a 1 pg per 10 mL (average, 44.66 ± 1.52 nF) DNA concentration of *E. coli* O157:H7 ATCC 43895. The analyses of the small capacitance change responses of 3.3 ± 0.75 nF for *E. coli* MTCC 3221 and 1.06 ± 0.25 nF for *E. coli* O78:H11 MTCC 723 reveal that these capacitance responses were statistically insignificant compared with the capacitance change response to *E. coli* O157:H7 ATCC 43895 from the baseline measurements. Fig. 6 reveals *p*-values of 0.42 for a 0.1 pg per 10 mL analyte concentration of *E. coli* MTCC 3221 and 0.46 for a 1 pg per 10 mL analyte concentration of *E. coli* O78:H11 MTCC 723. In comparison, the *p*-values for 0.1 pg per 10 mL and 1 pg per 10 mL analyte concentrations of *E. coli* O157:H7 ATCC 43895 were found to be 0.03 and 0.006, respectively, from the baseline measurements. Hence, we concluded that these negligible cross-reactivities may have occurred due to a mismatch in the base-pairing of the complementary DNA targets with the DNA probe. Because capacitive sensing is highly sensitive to the development of net charges at the interface of DNA hybridization,[49] changes in the capacitance responses for 0.1 pg per 10 mL and 1 pg per 10 mL DNA targets of *E. coli* MTCC 3221 and *E. coli* O78:H11 MTCC 723, respectively, were observed. These capacitance variations probably occurred due to a net charge increase at the interface, which could not replace the solvent molecules present on the ZEC sensor chip surface during the time of DNA–DNA interaction. This phenomenon occurred near the sensor surface during the time of measurement; it can be attributed to the specificity of the *z3276* DNA probe and the insulation of the ZEC sensor chip surface toward non-specific adsorption of DNA targets from *E. coli* MTCC 3221 and *E. coli* O78:H11 MTCC 723. Notwithstanding the negligible cross-reactivity, as mentioned in the previous section, no cross-reactivity of the developed ZEC sensor chip was detected when DNA from *B. subtilis* MTCC 736 (0.1, 1 and 10 pg per 10 mL) was tested.

4. Conclusions and future horizons

Surveillance of water-borne disease outbreaks due to poor water quality is required in a timely manner to save human lives. Therefore, in the present work, a highly sensitive, novel capacitive z3276 genetic marker-based ZEC sensor chip for the sensitive detection of *E. coli* O157:H7 in water was developed. The fabricated ZEC sensor chip was characterized by EIS, AFM, SEM, and percentage of pinholes. The results obtained in our study demonstrate a systematic declining trend of the capacitance value upon DNA hybridization. The ZEC sensor chip for *E. coli* O157:H7 exhibited a linear capacitance change response in the 0.5 to 25 pg per 10 mL range with a LOD of 13.67 CFU per 10 mL (equivalent to 0.1 pg per 10 mL). Moreover, the fabricated ZEC sensor chip did not yield any significant cross-reactivity with *E. coli* MTCC 3221, *E. coli* O78:H11 MTCC 723 or *B. subtilis* MTCC 736; hence, we found the developed ZEC sensor chip to be highly specific for sensitive detection of *E. coli* O157:H7. Due to the sensitivity and specificity of reported DNA-based sensing probes, these sensors have potential for practical use and commercialization as point-of-care-devices. DNA sensors fabricated on conducting substrates such as ITO can be miniaturized using the microfabrication process and the non-conventional electrode fabrication process. However, one of the key obstacles to DNA-based diagnostics is upstream processes such as DNA extraction and DNA denaturation prior to the detection of DNA hybridization. In future, a key challenge will be to develop a DNA sensor for the detection of pathogens without prior concentration steps for lab-on-chip applications.

Conflicts of interest

The authors declare that they do not have any conflicts of interest.

Acknowledgements

We are sincerely thankful to the Indian Council of Medical Research (ICMR) for a Senior Research Fellowship to Mr Rehan Deshmukh. The aminated DNA probe and primer set were procured from the host institute's Annual Contingency Funds sanctioned to Professor Utpal Roy. The work was partly funded by a CORE-WWEM grant of BITS Pilani. DST-FIST funding support for the AFM facility at the Department of Chemistry is duly acknowledged.

References

1 A. K. Deisingh and M. Thompson, *J. Appl. Microbiol.*, 2004, **96**, 419–429.
2 S. M. Chekabab, J. Paquin-Veillette, C. M. Dozois and J. Harel, *FEMS Microbiol. Lett.*, 2013, **341**, 1–12.
3 N. Kumar, Y. Hu, S. Singh and B. Mizaikoff, *Analyst*, 2018, **143**, 359–373.
4 A. M. Lupindu, *South. Afr. J. Infect. Dis.*, 2018, **33**, 24–30.
5 S. A. Kushon, K. D. Ley, K. Bradford, R. M. Jones, D. McBranch and D. Whitten, *Langmuir*, 2002, **18**, 7245–7249.
6 F. Azek, C. Grossiord, M. Joannes, B. Limoges and P. Brossier, *Anal. Biochem.*, 2000, **284**, 107–113.
7 E. Fortin, P. Mailley, L. Lacroix and S. Szunerits, *Analyst*, 2006, **131**, 186–193.
8 H. A. Ferreira, F. A. Cardoso, R. Ferreira, S. Cardoso and P. P. Freitas, *J. Appl. Phys.*, 2006, **99**, 08P105.
9 V. Stambouli, M. Labeau, I. Matko, B. Chenevier, O. Renault, C. Guiducci, P. Chaudouët, H. Roussel, D. Nibkin and E. Dupuis, *Sens. Actuators, B*, 2006, **113**, 1025–1033.
10 J. S. Daniels and N. Pourmand, *Electroanalysis*, 2007, **19**, 1239–1257.

11 M. H. Le, C. Jimenez, E. Chainet and V. Stambouli, *Sensors*, 2015, **15**, 10686–10704.
12 X. Chen, C. Liu, M. D. Hughes, D. A. Nagel, A. V Hine and L. Zhang, *J. Biosens. Bioelectron.*, 2015, **6**, 173.
13 W. Yang, J. E. Butler, J. N. Russell and R. J. Hamers, *Langmuir*, 2004, **20**, 6778–6787.
14 M. Lazerges and F. Bedioui, *Anal. Bioanal. Chem.*, 2013, **405**, 3705–3714.
15 W. A. Lai, C. H. Lin, Y. S. Yang and M. S. C. Lu, *Biosens. Bioelectron.*, 2012, **35**, 456–460.
16 K. Rijal and R. Mutharasan, *Analyst*, 2013, **138**, 2943.
17 C. Gautier, C. Cougnon, J. F. Pilard and N. Casse, *J. Electroanal. Chem.*, 2006, **587**, 276–283.
18 C. Tlili, N. J. Jaffrezic-Renault, C. Martelet and H. Korri-Youssoufi, *Mater. Sci. Eng., C*, 2008, **28**, 848–854.
19 P. Li, X. Wang, W. Gao, W. Yan, W. Guan, Y. Ma, Y. Yu, F. Ji, S. Wu and K. Ding, *Analyst*, 2018, **143**, 1462–1467.
20 M. K. Patel, J. Singh, M. K. Singh, V. V. Agrawal, S. G. Ansari and B. D. Malhotra, *J. Nanosci. Nanotechnol.*, 2013, **13**, 1671–1678.
21 A. Ramanaviciene and A. Ramanavicius, *Anal. Bioanal. Chem.*, 2004, **379**, 287–293.
22 V. Ratautaite, S. N. Topkaya, L. Mikoliunaite, M. Ozsoz, Y. Oztekin, A. Ramanaviciene and A. Ramanavicius, *Electroanalysis*, 2013, **25**, 1169–1177.
23 M. Z. H. Khan, *Cogent Eng.*, 2016, **3**, 1170097.
24 O. Simoska and K. J. Stevenson, *Analyst*, 2019, **144**, 6461–6478.
25 I. Tiwari, M. Singh, C. M. Pandey and G. Sumana, *Sens. Actuators, B*, 2015, **206**, 276–283.
26 B. Xu, D. Zheng, W. Qiu, F. Gao, S. Jiang and Q. Wang, *Biosens. Bioelectron.*, 2015, **72**, 175–181.
27 N. T. Perna, G. Plunkett, V. Burland, B. Mau, J. D. Glasner, D. J. Rose, G. F. Mayhew, P. S. Evans, J. Gregor, H. A. Kirkpatrick, G. Pósfai, J. Hackett, S. Klink, A. Boutin, Y. Shao, L. Miller, E. J. Grotbeck, N. W. Davis, A. Lim, E. T. Dimalanta, K. D. Potamousis, J. Apodaca, T. S. Anantharaman, J. Lin, G. Yen, D. C. Schwartz, R. A. Welch and F. R. Blattner, *Nature*, 2001, **409**, 529–533.
28 R. A. Deshmukh, S. Bhand and U. Roy, *Anal. Methods*, 2019, **11**, 3155–3167.
29 R. Deshmukh, S. Bhand and U. Roy, *Braz. J. Microbiol.*, 2019, DOI: 10.1007/s42770-019-00161-8.
30 A. Shrivastava and V. Gupta, *Chron. Young Sci.*, 2011, **2**, 21.
31 A. K. Prusty and S. Bhand, *Electroanalysis*, 2017, **29**, 1867–1875.
32 A. Mahadhy, E. Ståhl-Wernersson, B. Mattiasson and M. Hedström, *Biotechnol. Rep.*, 2014, **3**, 42–48.
33 S. Campuzano, M. Pedrero, C. Montemayor, E. Fatás and J. M. Pingarrón, *J. Electroanal. Chem.*, 2006, **586**, 112–121.
34 A. K. Prusty and S. Bhand, *Electroanalysis*, 2019, **31**, 1797–1808.
35 M. A. Aziz, S. Patra and H. Yang, *Chem. Commun.*, 2008, 4607.
36 C. Berggren, B. Bjarnason and G. Johansson, *Electroanalysis*, 2001, **13**, 173–180.
37 V. Tsouti, C. Boutopoulos, I. Zergioti and S. Chatzandroulis, *Biosens. Bioelectron.*, 2011, **27**, 1–11.
38 A. Ramanavicius, A. Finkelsteinas, H. Cesiulis and A. Ramanaviciene, *Bioelectrochemistry*, 2010, **79**, 11–16.
39 M. L. S. Mello and B. C. Vidal, *PLoS One*, 2012, **7**, e43169.
40 M. K. Patel, P. R. Solanki, S. Seth, S. Gupta, S. Khare, A. Kumar and B. D. Malhotra, *Electrochem. Commun.*, 2009, **11**, 969–973.
41 V. Velusamy, K. Arshak, O. Korostynska, K. Oliwa and C. Adley, *Biotechnol. Adv.*, 2010, **28**, 232–254.
42 Y. Wang, J. Ping, Z. Ye, J. Wu and Y. Ying, *Biosens. Bioelectron.*, 2013, **49**, 492–498.
43 J. Wan, J. Ai, Y. Zhang, X. Geng, Q. Gao and Z. Cheng, *Sci. Rep.*, 2016, **6**, 19806.
44 D. Lin, R. G. Pillai, W. E. Lee and A. B. Jemere, *Microchim. Acta*, 2019, **186**, 1–9.
45 C. Ruan, L. Yang and Y. Li, *Anal. Chem.*, 2002, **74**, 4814–4820.
46 L. Yang, Y. Li and G. F. Erf, *Anal. Chem.*, 2004, **76**, 1107–1113.
47 T. L. Panasyuk, V. M. Mirsky, S. A. Piletsky and O. S. Wolfbeis, *Anal. Chem.*, 1999, **71**, 4609–4613.
48 S. A. Bustin, V. Benes, J. A. Garson, J. Hellemans, J. Huggett, M. Kubista, R. Mueller, T. Nolan, M. W. Pfaffl, G. L. Shipley, J. Vandesompele and C. T. Wittwer, *Clin. Chem.*, 2009, **55**, 611–622.
49 J. G. Webster, G. Nabovati, Y. W. Zhu and M. Sawan, in *Wiley Encyclopedia of Electrical and Electronics Engineering*, John Wiley & Sons, Inc., Hoboken, NJ, USA, 2015, pp. 1–12.

